DEFECT CLASSIFICATION AND IMAGING WITH PHASE ARRAY TECHNIQUES

V. Schmitz, W. Gebhardt, F. Bonitz
Fraunhofer Institut für zerstoerungsfreie Pruefverfahren
Saarbrücken, West Germany

ABSTRACT

The use of arrays and the possibility of electronic beam steering, focusing and side lobe suppression allows a better defect classification and reconstruction of defective areas in work pieces, components and industrial plants. Because of synthesizing a large sector by a narrow ultrasonic beam, the advantage of a narrow beam for good signal/noise ratio is combined with the advantage of a broad beam for good detectability of unfavorable orientations of flaws. A Fortran program has been written for an equidistant or nonequidistant linear array with the arbitrary choice of amplitude and phase of each element. For shear wave excitation, the shear wave point characteristic of a point source is implemented. The phased array technique has been used for distinction between cracks and voluminous flaws and for the destination of flaw inclination and surface curvature. Three evaluation methods can be used: interpretation of the sector display; generation of compound-scan amplitude locus curves, and flaw imaging by superposition of all sector scans on a storage display. The experimental results show that the arrays are a powerful tool in increasing the reliability of nondestructive testing methods.

INTRODUCTION

One of the central points in nondestructive evaluation (NDE) is the flaw analysis, i.e., the determination of shape, size and orientation of defects. Especially, the distinction between cracks and voluminous defects is of great importance. The flaw size is usually estimated by echo height assessment related to the equivalent disc reflector which is oriented perpendicularly to the acoustic axis of the probe. A more far reaching defect characterization is possible by evaluating amplitude locus curves (AOK) which are generated by recording the echo height versus probe position. Classification by such methods has been done until now with only simple model reflectors. Flaws which are large in comparison with the beam diameter can be measured by scanning, however, there is a high probability that the beam is deflected and only flaw edges are recognized. New methods for defect classification and reconstruction arise by using electronically steerable array probes. It is possible to influence the sound field on a large scale by changing the insonification angle, beam diameter, ratio between main lobe and side lobes or to synthesize a large sector by steering a narrow sound beam. The dynamic movement of an image when moving the probe along the surface gives additional information.

To check all these possibilities, a modified medical phased array system has been used. The system operates at 2 MHz and the focus can be varied within the nearfield of a 20 element probe. The effect of the dimensions of the elements of such an array, together with acoustical coupling effects, has been calculated and used for the design of optimized probes.

CALCULATION OF ARRAY BEAM PATTERNS

For the calculation of the beam patterns, the basic Huyghen's principle is used. It is assumed that the single elements of the array are arranged in one line but the distance between two elements can be equidistant or nonequidistant. Each element may be individually excited in amplitude and phase. The program calculates the intensity of one component of particle displacement. For longitudinal waves, it is the normal particle displacement and for shear waves, the tangential displacement in a distance z. The particle displacement can be calculated for up to 500 different points in a constant distance z or in a fixed radius from the array center. Amplitudes, phases and number of elements must be within 100.

With S_{1k} the position of one element, R_{1k} the distance to a field point A(x,y,z), and β_{1k} the corresponding angle to this field point are complex added:

$$u(A(x,y,z)) = \sum_{n}^{L} \sum_{k}^{M} \frac{1}{R_{nk}} e^{i(kR_{nk} - \phi_n)} u(\beta_{1k}) \quad (1)$$

with

L = number of array elements
M = number of division of each element
k = wave vector
ϕ = phase of each single element
u = particle velocity of a point source attached to a half space
R = directivity pattern.

The beam pattern of a point for longitudinal waves has been chosen according to Krautkraemer to $U_N = \cos\theta$ and for shear waves according to Miller/Pursey (Ref. 1).

$$u_T = \frac{\sin 2\theta \sqrt{\mu^2 \sin^2\theta - 1}}{F(\xi)} \quad (2)$$

$$\xi = \mu \sin\theta \quad (3)$$

$$F(\xi) = (2\xi^2 - \mu^2)^2 - 4\xi^2 \sqrt{(\xi^2 - 1)} \cdot \sqrt{\xi^2 - \mu^2} \quad (4)$$

$$\mu^2 = \frac{2(1 - \nu)}{1 - 2\nu} \quad (5)$$

with

ν = Poisson's ratio

The directivity function calculates to:

$$R = u_N \cdot u_N^* \quad \text{or} \quad = u_T \cdot u_T^* \qquad (6)$$

The program has been written in Fortran, implemented on a PDP 11 and on a VAX. The basic structure is seen in Fig. 1:

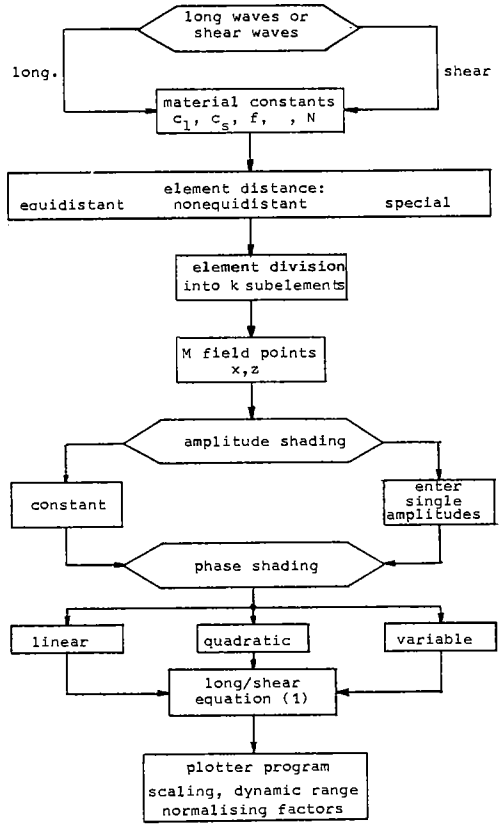

Fig. 1 Program used for the calculation of array beam pattern.

Key elements in array systems are the delay lines, modern equipment use charged coupled delay lines (CCD's). The delay time of these devices is proportional to aninternal clock frequency. The clock frequency is generated by a frequency synthesizer, which is a phase locked loop generator. The time this loop needs to stabilize depends on the accuracy of the frequency needed. The program has been used to calculate the array directivity pattern of an improperly steered array and calculations run for a 20 element array with elements distanced $\lambda/2$ both for longitudinal waves and for shear waves. We have found that instead of a 500 Hz step, a frequency step of 10 kHz is still allowable (Fig. 2(a) and (b).

The use of 100 kHz steps is not recommended because the effect is a second main lobe. Phase errors by use of the 10 kHz steps consist of small shifts in the main lobe of about 3° and a small shift in the distance to the side lobes.

Another application has been to calculate the effect of amplitude shading. Figure 3 shows a 16 element array with elements spaced $\lambda/2$ wave length

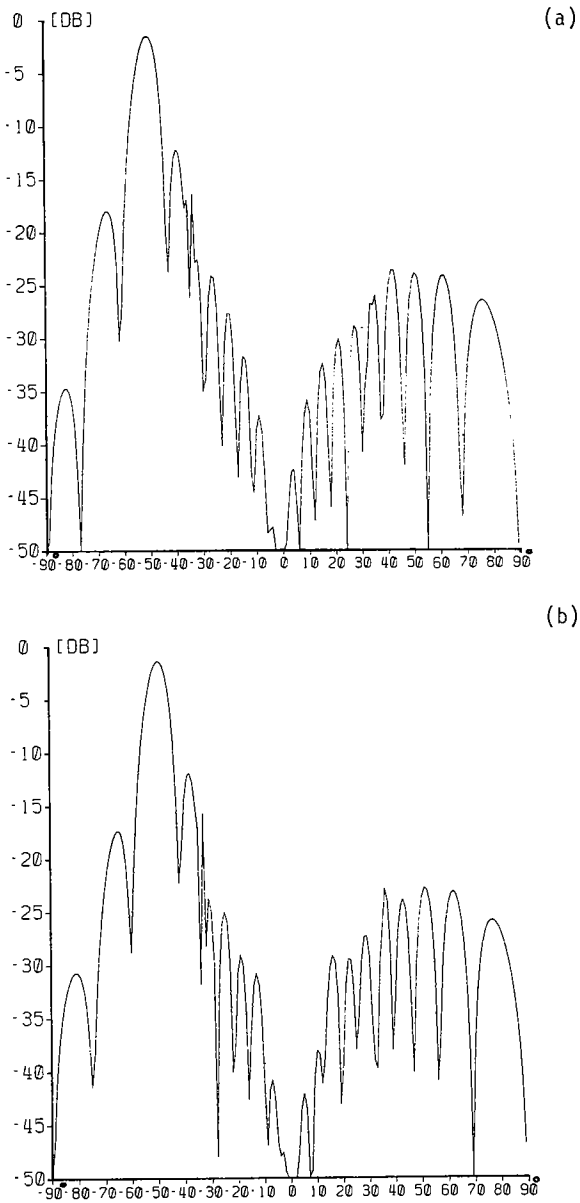

Fig. 2 Directivity pattern of a steered 50°, 20 element array with shear wave excitation. (a) 500 Hz clock frequency; (b) 10 kHz clock frequency.

apart, with and without Hamming weighting. The beam has been steered by 45°. The dotted line corresponds to the nonweighted array. The main lobe/side lobe distance is about 10 dB. The use of the amplitude shading increased this distance to about 25 dB.

A third application is the calculation of directivity patterns for arrays with nonconstant distances of the single elements. One possibility is the sin distribution:

$$s_i = \frac{L}{2N}\left(i + p.\sin\frac{2i\pi}{2N}\right) \qquad (7)$$

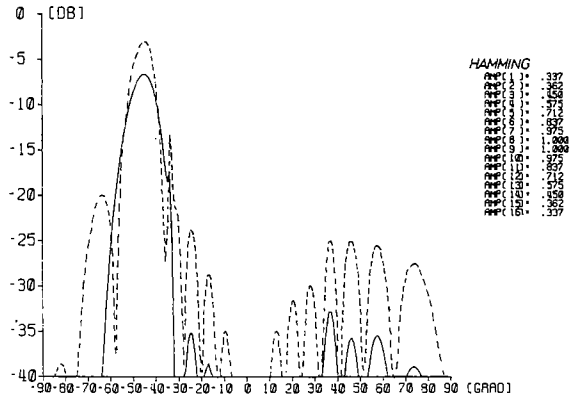

Fig. 3 Array-Shear-Wave-Beam-Pattern, 45° steered, with and without Hamming-weighting.

with S_i = distance of the i-th element to the midth of the array, L = array length, N = number of elements and p = coefficients. The p coefficients cause a narrower element distance in the middle of the array. For a 2 MHz, 11 element array the calculations are performed for an average element distance of 1.5, 0.5 and .75 wavelength. With a 1.5 wavelength element distance, the 11° steering of the array caused a main lobe/side lobe distance of only 4 dB. A weighting by Dolph-Tschebyscheff could increase this distance by only 0.5 dB. An element distance of 1 wavelength allowed a steering of 20° with 6.8 dB side lobe suppression and an improvement by 4 dB. An average element distance of 0.75 wavelength allowed a steering of 30°, with 5.5 dB and together with Dolph-Tschebyscheff shading of 10 dB. The calculations showed in this case, four elements can be saved when steering within 20°.

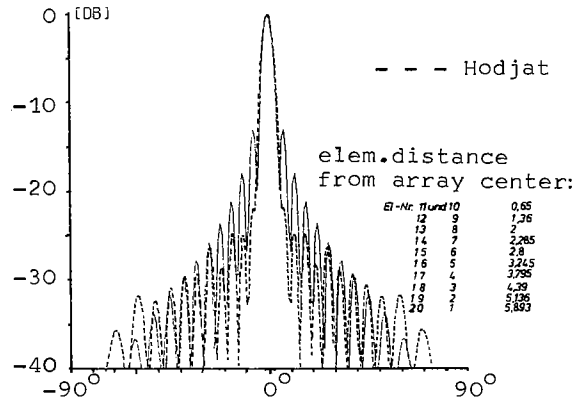

Fig. 4 Directivity pattern with 24 equally spaced elements compared with a 20 element array spaced according to Hodjat (Ref. 2).

DEFECT CLASSIFICATION AND RECONSTRUCTION BY SECTOR-SCANNING

If a scanning array probe is moved across the surface of a metal piece, the angle of maximum echo height changes from probe position to probe position. The position and the movement of an image point in a sector display is proportional to the position and the velocity with which the probe is moved. From the variation of the image, in time, intensity and position, conclusions can be drawn about the flaw parameters like shape, size and orientation. (Ref. 3,4).

First, we will discuss the case of an ideal curved reflector, represented by a cylindrical bore hole.

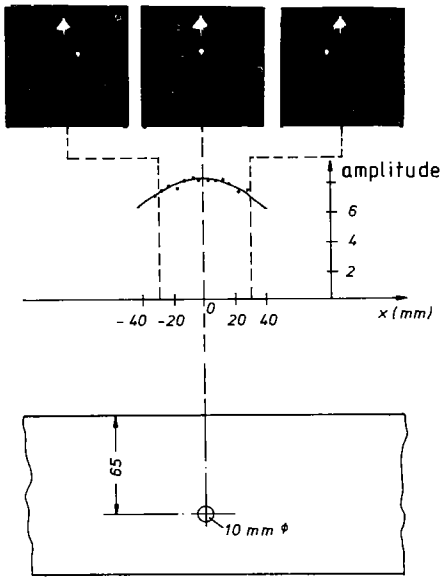

Fig. 5 Sector display and compound-scan-amplitude-locus curve of a curved reflector.

If the scanning probe is moved along the surface of the specimen from left to right, the image point moves across the total sector and finally disappears at the left. Since a curved reflector has no directivity, the intensity variation of the image point is small and is brightest in the middle of the sector equivalent to the smallest time-of-flight. This dynamic behavior allows us to tell this is a curved flaw.

Consider now the case of a planar defect, which is represented in Fig. 6 by a 10 mm flat bottom hole with 30° inclination.

Because a flat reflector has a pronounced directivity, the image point will not move across the whole sector but rather over a short distance. The orientation of the reflector is equal to the orientation of the scan line running through the brightest spot. This is totally different behavior compared to a curved flaw and indicates the inclination of a planar flaw.

DEFECT CLASSIFICATION AND RECONSTRUCTION BY COMPOUND SCAN AMPLITUDE LOCUS CURVE VAOK

A more quantitative description of the flaw parameters is possible by means of a compound scan amplitude locus curve (VAOK) which is generated by recording the maximum echo amplitudes versus the corresponding array probe positions according to Fig. 5 and 6. Because the center of the array

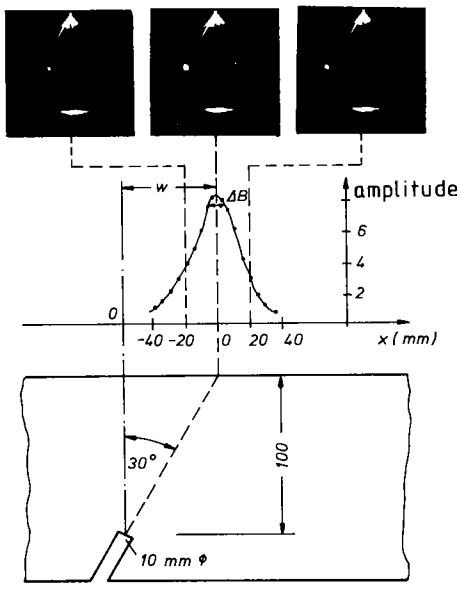

Fig. 6 Sector display and compound-scan-amplitude-locus curve of a planar defect.

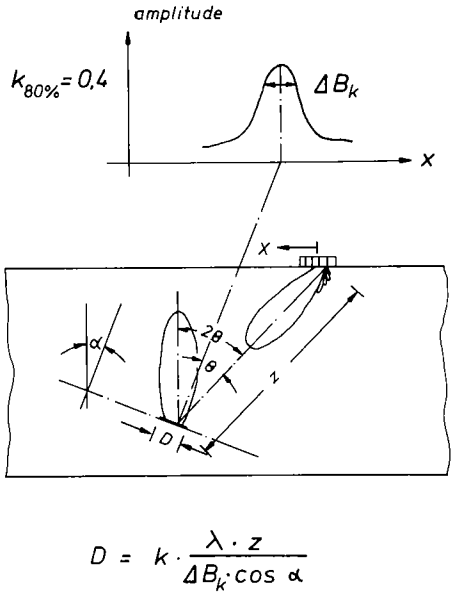

$$D = k \cdot \frac{\lambda \cdot z}{\Delta B_k \cdot \cos \alpha}$$

Fig. 7 Relationship between compound-scan-amplitude-locus curve and flaw size D.

beam looks always toward the flaw, the probe characteristic is eliminated automatically. The compound scan amplitude locus curve depicts directly the directivity function of the flaw. In the case of the cylindrical bore hole in Fig. 5, the locus curve reaches a maximum just above the reflector and diminishes slowly to the left or right.

The planar reflector (Fig. 6) maximum amplitude occurs in a position where the ultrasonic beam is incident and perpendicular to the reflector plane. Now the maximum of the locus curve is not just above the reflector but rather shifted by a distance w. The maximum shift which depends upon inclina tion and flaw depth, besides the shape of the curve, is an important criterion to distinguish between curved and planar defects. From the position of the maximum and the measured flaw depth, the orientation can be determined.

Figure 7 shows the relation between the directivity of a planar reflector and the compound scan amplitude locus curve. Here α is the flaw angle reference to the surface, ΔB the width of the amplitude locus curve, λ the wavelength and z the distance between reflector and probe position. k is a factor depending on the level where the width of the curve is measured. If the width is measured at 80% of its maximum value, k = 0.4.

DEFECT CLASSIFICATION AND RECONSTRUCTION BY COMPOUND SCANNING

The principle of this evaluation method, known for several years in medical diagnostics, is a combination of a sector display and the lateral movement of an array probe. In one probe position, a full sector scan is performed and stored in a storage display or a digital scan converter. Then the probe is moved a distance and the correspondent sector scan is stored but shifted proportional to the array-probe movement. This gives a highly accurate image of an irregular shaped flaw because the probe has a height acceptance angle of about 90°, which is synthesized by steering a focused narrow beam.

In the following, some examples for compound scan imaging are presented. Figure 8 shows the image of a 12 mm side drilled hole in a 150 mm thick specimen at a depth of 100 mm. Surface, back wall, depth of the side drilled hole and its shape are clearly visible. In addition, the figure shows the image of a bottom hole at a 100 mm depth where the cone of 32° and the 20 mm diameter can be read out immedately.

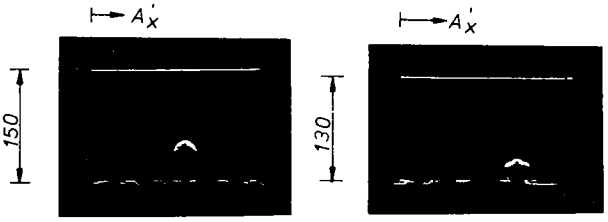

Fig. 8 Compound scan imaging of a cylindrical side drilled hole and a bottom hole with 32° cone.

Figure 9 shows imperfect homogeneous layers in a 300 mm steel specimen. Position and orientation of the layers are evident. Figure 10 shows cross sections of the weld zone in a 1400 x 800 x 200 mm^3 specimen with natural cracks in it. The picture shows front surface, back surface root of the weld, shape and curvature of the cracks. Crack height to 2/3 of the specimen's thickness can be recognized. After destructing the specimen, the true profile could be compared with the measured depth profile. A good agreement was achieved.

The compound scan imaging can be improved to a "roundabout scanning", and in Fig. 11 the flaw

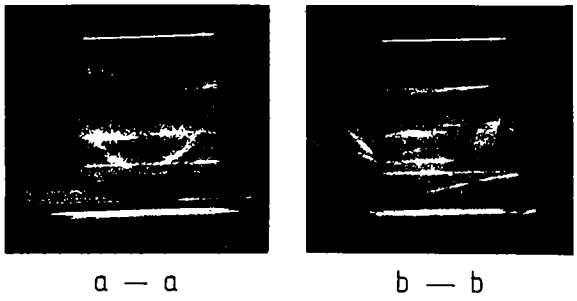

Fig. 9 Compound scan imaging of inhomogeneities in a steel specimen.

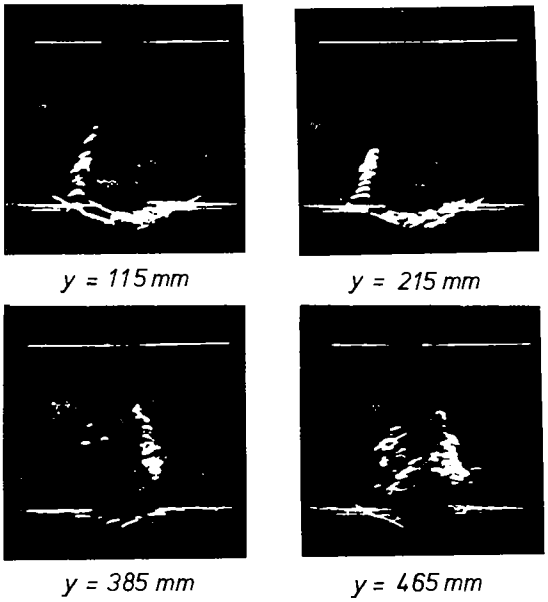

Fig. 10 Compound scan imaging of natural cracks in a weld.

echoes reflected via the backwall are recorded. In this way, not only the upper surface of the defect is reconstructed but also its underside.

CONCLUSIONS

A computer program has been developed which calculates the directivity pattern of a linear array with arbitrarily spaced elements, with free choice of amplitude and phasing of each element. It was shown that the electronic sector and compound scan based upon phased array beam forming techniques is a powerful tool for the flaw analysis. We are convinced that these methods are an important step to distinguish between curved defects and cracks.

ACKNOWLEDGMENTS

This work is supported by the Federal Ministry of Research and Technology within the scope of reactor safety research program.

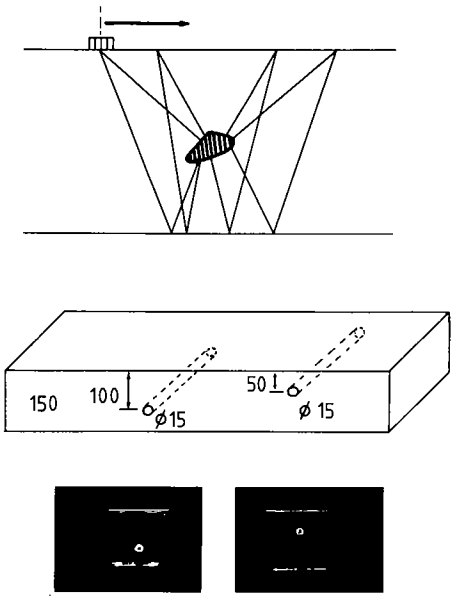

Fig. 11 Compound scan imaging improved to a roundabout scanning.

REFERENCES

1. Miller/Pursey, "The Field and Radiation Impedance of Mechanical Radiators on the Free Surface of a Semi-infinite Isotropic Solid," Proc. Roy. Soc., London, A223, 1954, pp. 521-541.

2. Hodjat, F., Horanessian, S.A., "Nonuniformly Spaced Linear and Planar Array Antennas for Sidelobe Reduction IEEE Transaction on Antennas and Propagation," Vol. AP-26, March, 1978.

3. Gebhardt, W., Bonitz, F., Woll, H., Schmitz, V., "Beam Forming and Defect Characterization by Phased Array Systems," Proc. of Ninth World Conference on NDT, Melbourne, 1979, Paper 4FFD-1.

4. Gebhardt, W., Bonitz, F., Woll, H., Schmitz, V., "Determination of Crack Characteristics Size and Orientation of Defects by Phased Array Technique in NDT," NDE In Nuclear Industry, 11-14.2.80, Salt Lake City, Utah.

Gordon Kino, Chairman (Stanford University): There is time for one or two questions.

Unidentified Speaker: Did you do any samples where the range to the flaw was on the order of magnitude larger than that compared to the flaw size? It looked like the range was about on the order of 10 times the size of the flaw. Did you do any situations where the range was on the order of a hundred times the size of the flaw? Do you have any such samples?

W. Gebhardt (Institute for NDT, Saarbruecken): Some flaw sizes have been two millimeters or three millimeters. The thickness of the specimen is 200 millimeters. I don't understand your question, because the range of the depth of the flaws has been more than 10 times greater than the actual sizes of the flaws.

Unidentified Speaker: The ones you showed were around 10. Were there any that that you did that were around a hundred times?

W. Gebhardt: Not in this sample. But this is the easiest way to do it. It's much more complicated to go below the depths of the flaws.

Unidentified Speaker: So there were other problems when you do that?

W. Gebhardt: You have a divergency of your actual sound beam, so what you lose is a solution probability because it can only focus within the near view length of a pole, and you have enough signal to noise ratio for imaging the complete specimen. What we have here are homogeneous materials. What depths are you thinking about?

Unidentified Speaker: On the order of 50 to a hundred times, and then the inhomogeneity of the medium becomes a greater issue as well as the problems in resolution in the beam itself and the spreading of the beam so that what happens is time doesn't translate into range as easily as you move across this scan, and you don't get that nice -

Gordon Kino, Chairman: Next question.

Bob Addison (Rockwell Science Center): You said that you operated with two megahertz. I wonder that the length of your transient response was of the transducer probe.

Gordon Kino, Chairman: It's about three rf cycles.

Jack Smith: You showed a simulation of a sparse array as an equally spaced element. Did you actually use such an array to make some of the images you showed?

W. Gebhardt: We did not use this array for this image as shown. We have one in our institute but not yet the time for using it on experiments, so perhaps I can give you more details in about a half a year. But it shows to have varied the restrictions if you steer the beam more than 45 degrees.

Gordon Kino, Chairman: So was this the array that was used here; how many elements were used?

W. Gebhardt: Twenty elements equally spaced.

Gordon Kino, Chairman: Equally spaced. And then it was moved along mechanically?

W. Gebhardt: It was gently moved along with the hand-held camera I showed you in the first pictures.

Gordon Kino, Chairman: One more question.

Unidentified Speaker: Did you see any artifacts due to mode conversion?

W. Gebhardt: Yes, we can see this image. No, artifacts I didn't see. But what you can see are mode-converted longitudinal waves and the corresponding images of these mode-converted rays, but because of the different sound velocity and not affected element distance they have another angle in the image and to move velocity into dynamic movement, then the - . So you can't decide if this is an actual defect; longitudal wave or if it is a mode-converted wave which images the same point in space to another image point.

Unidentified Speaker: In the first couple of slides, one or two of the images had a white dot off to the side in various places. Were those mode images, or --

W. Gebhardt: This was a real image. The white dot? Was it the image or the slide?

Unidentified Speaker: I think it was in the second or third slide.

W. Gebhardt: This was the actual image.

Gordon Kino, Chairman: Thank you very much.